



Simulation of Flood Hazard Risk for Naban Reservoir Safety Management: A Comprehensive Assessment



Cheng Zhong¹, Rongcai Liang¹, Wenle Qin¹, Liting Cai^{2*}

¹ Naban Reservoir Management Center, Water Resources Department of Guangxi Zhuang Autonomous Region, 535599 Fangchenggang, China

² College of Civil Engineering and Architecture, Guangxi University, 530004 Nanning, China

* Correspondence: Liting Cai (16659470669@163.com)

Received: 06-15-2023

Revised: 07-20-2023

Accepted: 07-25-2023

Citation: C. Zhong, R. C. Liang, W. L. Qin, and L. T. Cai, "Simulation of flood hazard risk for Naban Reservoir safety management: A comprehensive assessment," *Acadlore Trans. Geosci.*, vol. 2, no. 3, pp. 132–144, 2023. <https://doi.org/10.56578/atg020301>.



© 2023 by the authors. Published by Acadlore Publishing Services Limited, Hong Kong. This article is available for free download and can be reused and cited, provided that the original published version is credited, under the CC BY 4.0 license.

Abstract: Safety of reservoir dams remains pivotal for societal stability, underscoring the significance of efficient emergency management strategies. This investigation focuses on Naban Reservoir, where the BREACH model was employed to simulate potential dam failures. By integrating one-dimensional and two-dimensional modeling approaches, a mathematical representation was developed to scrutinize flood progression in the adjacent region. Correlation coefficients for the devised model ranged from 0.945 to 0.986, with relative errors of -13.72%, -0.23%, -17.41%, and -15.44%. Comparisons indicated that observed flow rates align closely with simulated rates. Notably, significant land slippages surrounding the reservoir were not detected, implying that an enhanced downstream surge due to an upstream collapse is unlikely. Nevertheless, a breach in the main dam could result in catastrophic outcomes for downstream zones, particularly affecting infrastructure and communities along the Shangsi and Zaimiao Basins. Critical observation zones, such as Siyang Town in Shangshi County, Zaimiao Town in Shangshi County, and Nakan Town in Ningming County, were identified, emphasizing the need for enhanced precautionary measures to safeguard human lives, property, and societal stability. This research has paved the way for a novel flood early warning system tailored for the Naban Reservoir, ensuring timely predictions and alerts. Such advancements augment the disaster prevention capacity, offering valuable insights for mitigating risks in small to medium-sized reservoirs.

Keywords: Flood hazard; Reservoir safety; One-dimensional modeling; Two-dimensional modeling; Dam breach

1 Introduction

Situated within a monsoon climate zone, China is routinely subjected to high rainfall intensities during the flood season. Consequently, floods are recognized as the most prevalent natural disasters in the region [1]. The grave threat they pose to the safety of life and property underscores the imperative of flood prevention and mitigation measures [2–4].

Central to these mitigation strategies are reservoirs, pivotal hydraulic infrastructures, designed with three-fold functionality: flood control, water supply, and irrigation. Yet, a concerning observation has been made. Many existing reservoirs, having been constructed several years ago, now fall short of current flood risk management standards, presenting numerous safety hazards. In the unfortunate event of dam failures following flood disasters, the resultant devastation in downstream regions can be monumental [5, 6].

The potential severity of these consequences has led to the institution of specialized early warning systems. These systems are believed to considerably enhance the safety profile of reservoirs, concurrently reducing their vulnerability to water hazards, thus contributing significantly to disaster prevention and mitigation [7–9]. Enabled by advanced GIS technology, artificial intelligence, and machine learning techniques, these early warning systems adeptly analyze vast flood datasets, facilitating real-time flood prognostications [10, 11]. A notable impact of such systems is evident in certain underdeveloped nations where significant declines in mortality rates, attributable to natural calamities, have been recorded following the implementation of flood early warning systems [12]. Emphasizing their importance, the establishment of technology-aided flood early warning systems is now prioritized in flood prevention and mitigation agendas [13, 14].

Integral to these systems is the ability to undertake quantitative flood hazard risk evaluations and devise strategies for hazard minimization [15, 16]. The undertaking of flood hazard risk assessments is not only pivotal to flood risk management but also vital for reservoir safety governance [17, 18]. Several methods, ranging from the indicator system and historical flooding methods to hydrological-hydraulic model simulations, have been employed for these assessments [19–21]. However, it's noteworthy that the driving factors of floods—such as climate, hydrology, topography, land use, and soils—inject inevitable uncertainties into these evaluations, necessitating a multidimensional approach [22, 23]. The traditionally employed flood assessment methodologies, although comprehensive, often grapple with data insufficiencies and multiple constraints. Thus, a shift towards more pragmatic and streamlined flood models is discernible, with these models progressively superseding the conventional methods to deliver rapid and precise flood simulations [24–26]. Such advancements in early warning systems fortify reservoirs, enabling them to pre-empt water disasters, which, in turn, reinforces their safety management competencies.

A review of current literature reveals a range of models, including the MIKE series, SHUD, SWMM, and HEC-HMS, which have been utilized for simulating flood dynamics [27–30]. Several empirical studies serve as exemplars. For instance, in a study by Yang et al. [31], a hybrid model integrating SWMM and MIKE21 was developed to ascertain the implications of rainfall irregularities on urban flooding. Similarly, Barreiro et al. [32] harnessed a combination of one-dimensional SWMM and two-dimensional MOHID models, yielding a more nuanced urban flooding model that provided a better representation of stormwater effects. In a distinct effort, Wang et al. [33] extrapolated current and future river flood dispersions and localized flood inundations using the MIKE FLOOD model, affirming its potential in guiding the scientific planning of urban infrastructures. Furthermore, Lu et al. [34] relied on the MIKE FLOOD model to execute a quantitative analysis of present-day land use, topographical parameters, and flood containment capacities, thereby offering invaluable technical backing for the digitization and precision-targeted watershed flood management.

However, a glaring research gap persists. While flood modeling research predominantly targets urban or flat terrains, scant attention has been accorded to its application in the domains of reservoir water hazard risk and safety management. This oversight is particularly concerning given the vast populations whose lives and assets are intertwined with the safety of these reservoirs. Addressing this deficit, the present study endeavors to provide a meticulous quantitative assessment of the flood dynamics of the Naban Reservoir, especially under dam failure scenarios. The research focus is centered on the Naban Reservoir, strategically located in the Ming River's mainstream. Employing a combination of one-dimensional (MIKE11 river network model) and two-dimensional (MIKE21 surface model) coupled models, flood inundations under varying flood magnitudes are simulated. The fusion of these models aims to comprehensively capture the hydrological nuances of the reservoir's surrounding basin, ensuring superior simulation accuracy. Concurrently, the study introduces a reservoir flood warning model, synthesized using the aforementioned coupled models, to facilitate real-time flood predictions, thereby bolstering reservoir disaster prevention and mitigation capabilities.

In summation, this research is poised to furnish valuable data insights and scientific references, potentially guiding reservoir water hazard risk studies and shaping reservoir emergency strategy formulations.

2 Geographical and Climatic Profile of the Naban Reservoir Area

Naban Reservoir is situated within Shangsi County of Fangchenggang City, in the Guangxi Zhuang Autonomous Region. It is geographically positioned at 108°00' E longitude and 22°08' N latitude, as delineated in Figure 1. Nestled in the Ming River basin — the predominant tributary of the Zuojiang River basin — the reservoir is strategically located in the upper reaches of the Ming River [35].

The Ming River has its origins at the northern foothills of Guangxi's 100,000 mountains. It courses from the southwest to the northeast, spanning a distance of 315 km, and draining a watershed area encompassing 6379 km². Notably, the Tuolin River, the Gongan River, and the Pailian River are identified as its principal tributaries. The watershed experiences a subtropical monsoon climate, characterized by ample precipitation and sunshine. Within the basin, an average annual temperature of 21.3°C is recorded. Additionally, an average annual evaporation of 1,647 mm and a relative humidity of approximately 81 percent are observed.

Flowing through multiple townships in Fangchenggang City, including Shangsi County, Si Yang, and Jiao An, the Ming River basin sustains a populace exceeding one million. It envelopes over 400,000 acres of cultivated land and is critical for the protection of vital infrastructures such as the 100 km stretch of the Xianggui Railway and 3 km of the 311 Provincial Highway. Shangsi County, where the reservoir is anchored, is renowned for its bountiful natural resources, being designated as both a forestry and sugar-producing county.

Primarily established for irrigation, Naban Reservoir also facilitates power generation and urban water supply. Historically, it has been assailed by numerous typhoon events and flooding hazards, leading to considerable damages both to governmental infrastructure and the local populace, as cataloged in Table 1. Essential technical parameters of the reservoir, encompassing watershed area, multi-year average rainfall, multi-year average runoff, characteristic water level, and reservoir capacity, are detailed in Table 2. These parameters are subsequently employed as

foundational data during the modeling phase.

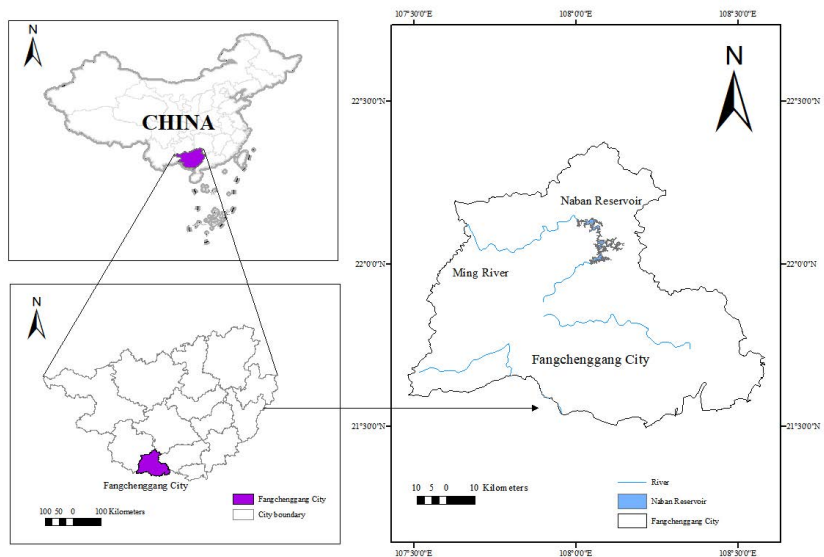


Figure 1. Schematic representation of the study area

Table 1. Historic records of significant flood events

Starting Moment	End Moment	Rising Water Level (m)	Maximum Water Level (m)	Average Rainfall in Reservoir Area (mm)	Flood Peak Flow (m^3/s)	Total Amount of Flood Water (billion m^3)
1994 – 7 – 14 18 : 00	1994 – 7 – 23 4 : 00	211.09	219.88	476	1300	2.3
1997 – 8 – 22 8 : 00	1997 – 8 – 27 8 : 00	213.99	219.72	356	3600	1.7
1998 – 6 – 25 6 : 00	1998 – 7 – 8 8 : 00	208.98	220.59	643	2300	3.0
2001 – 7 – 2 2 : 00	2001 – 7 – 4 12 : 00	215.81	222.76	457	4009	2.5
(Pearl River Basin above, Yellow Sea Basin below)						
2013 – 11 – 10 5 : 00	2013 – 11 – 12 5 : 00	219.63	222.64	334	3200	1.2
2014 – 9 – 8 6 : 00	2014 – 9 – 20 22 : 00	215.15	221.2	441	3800	2.1

Table 2. Principal technical indicators of Naban Reservoir (Utilizing the 1985 national datum elevation)

Name	Unit	Numerical Value
Watershed area	km^2	490
Multi-year average rainfall	mm	1229
Multi-year average runoff	m^3	63072×10^4
Normal water storage level	m	220.57
Design Flood Level	m	227.98
Calibration flood level	m	229.68
Stagnant water level	m	209.57
Dead storage capacity	m^3	1.64×10^8
Flood control reservoir capacity	m^3	4.00×10^8
Xingli storage capacity	m^3	2.64×10^8
Total storage capacity	m^3	8.28×10^8

3 Methodology: Model Construction and Validation

3.1 Hydrodynamic Model Construction

Given the intricate terrains present in the Ming River basin, encompassing forests, grasslands, clearings, settlements, and roadways, a flood simulation model has been developed, integrating both one- and two-dimensional modules. The one-dimensional module serves as the river network model, whereas the two-dimensional module functions as the terrestrial surface representation.

Within this context, the riverine flooding of the Ming River is depicted through the one-dimensional model, while the two-dimensional model emulates the inundation and lateral flow patterns adjacent to the riverbanks. To enhance the accuracy of riverine flood representation, and the complex terrains within the Ming River basin of the Naban Reservoir, the coupling of MIKE11 and MIKE21 was employed. This coupling optimally captures the hydrodynamics of the river and the surrounding terrain, aiming to diminish discrepancies between simulated and observed phenomena.

The underlying mathematical representation is rooted in the one-dimensional non-constant flow Saint-Venant equation set, which facilitates the depiction of the river's flow state. Generated outputs from this model encompass pivotal data such as inundation depths, flow rates, and velocities, which subsequently are utilized to formulate flood risk maps.

The governing Saint-Venant equations are articulated as:

$$\frac{\partial A}{\partial t} + \frac{\partial Q}{\partial x} = q \quad (1)$$

$$\frac{\partial Q}{\partial t} + \frac{\partial}{\partial x} \left(\frac{Q^2}{A} \right) + gA \frac{\partial h}{\partial x} + g \frac{Q}{C^2} \frac{|Q|}{AR} = 0 \quad (2)$$

where, A denotes the cross-sectional area (m^2), Q represents the flow rate (m^3/s), x signifies the distance coordinate (m), t is the time coordinate (s), h refers to the water level (m), q is the lateral inflow rate (m^3/s), C is associated with the Xie Cai coefficient, R stands for the hydraulic radius (m), and g encapsulates gravitational acceleration (m^3/s).

3.2 Boundary Conditions and Dam-Breach Scenarios

3.2.1 Influencing factors and dam-failure scenarios

Reservoir dam failures can be attributed to various causative agents such as extreme flood events, inadequacies in reservoir scheduling management, and seismic activities surpassing anticipated intensities. Through the analysis of dam-breach operations, breach modeling, and discharge computations, speculative insights into the reservoir breach format can be formulated. In this study, two primary dam-failure flood scenarios were deliberated upon. The initial scenario postulated a high-water level of 229.68m due to a 5000-year calibration flood, which, compounded with abnormal water seepage, led to an external slope failure. Conversely, the second scenario proposed dam failure at a normal storage elevation of 220.57m due to abrupt incidents.

3.2.2 Model parameters and computation

Naban Reservoir's dam, a homogenous construct of earth and rock, undergoes progressive breaches. For the estimation of such gradual dam breaches, the BREACH model was employed. Fundamental parameters of the reservoir were incorporated into this model (refer to Table 3). These parameters, when juxtaposed with the water level-reservoir capacity relationship curve (Figure 2), enabled the derivation of the dam-break flow process for Naban Reservoir, as depicted in Figure 3.

Following a thorough analysis of the dam-breach flow process, it was discerned that the peak flood flow for the first scenario amounted to 128,000 m^3/s , whilst the second scenario culminated in a peak flow of 80,000 m^3/s . Notably, the peak for the first scenario exceeded that of the second. Furthermore, the peak flow for the first case was attained at 1.5 hours, whereas the second scenario reached its zenith at 2.0 hours, rendering a temporal difference of 0.5 hours for peak emergence. However, the propagation durations were found to be nearly identical.

In accounting for the direst potential outcome of a Naban Reservoir dam failure, the dam-failure flood trajectory was based on the calibration level of the first scenario. This trajectory was subsequently introduced as the open boundary condition for numerical computations. Emphasis was placed on contemplating the most adverse circumstances during the formulation of flood contingency plans. As a result, three computational scenarios were established in this study. Depending on reservoir inflow rates under varying frequencies, reservoir spillway discharge processes for 100-year, 500-year, and 5000-year intervals were delineated according to scheduling principles and in conjunction with antecedent hydrological computations of the reservoir. These values were introduced as the inflow boundary conditions for open boundary computations.

Table 3. Parameterisation of dam failure conditions

Working Condition 1		Working Condition 2		
Serial	Parameter Name	Parameter Value	Parameter Name	
1	Inlet flow (m^3/s)	2870	Inlet flow rate (m^3/s)	653
2	Water surface	229.68	Water surface	220.57
3	Reservoir capacity	7.89	Storage capacity	4.28
4	Elevation of the top	232.56	Elevation of the top of	232.56
5	Material density	2490.2	The density of dam	2490.2
6	The angle of internal friction of matter ($^\circ$)	30	The angle of internal friction of the dam material ($^\circ$)	30
7	Matter cohesion	13	The cohesion of dam	13
8	D_{50} (m)	1.1	D_{50} (m)	1.1
9	D_{30} (m)	1.12	D_{30} (m)	1.12

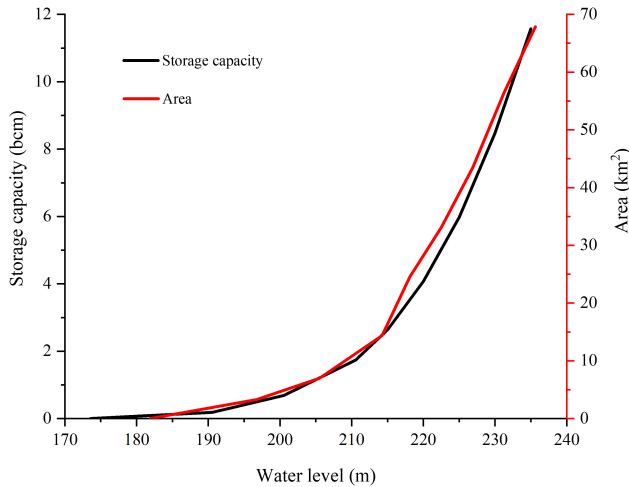


Figure 2. Water level-area-reservoir capacity relationship

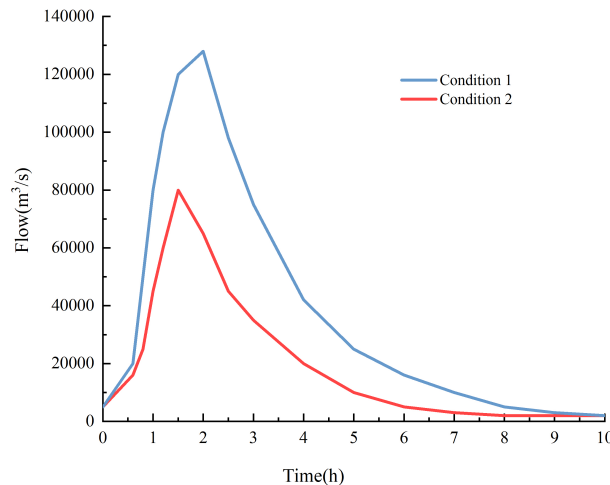


Figure 3. Process line of dam break flow under two operating conditions

3.2.3 Geographical boundaries and model inputs

The computational segment of Naban Reservoir's Ming River main course spans from the dam site to the concluding segment of the downstream Ming River Shangsi, a total expanse of 73,350 m (as shown in Figure 4). To

satisfy boundary prerequisites, it became essential to incorporate the configurations of power stations, gates, and dams situated throughout the river's course. Within the one-dimensional model of Naban Reservoir, upstream processes included flood discharge trajectories and dam-failure flows for each determined frequency. In contrast, downstream processes encapsulated the relationship between water level and flow. Time series files were generated from the flood discharge trajectories and dam-failure flows for each frequency, serving as upstream boundary conditions. Meanwhile, the downstream water level-flow relationship was directly input to the lower boundary, as tabulated in Table 4.

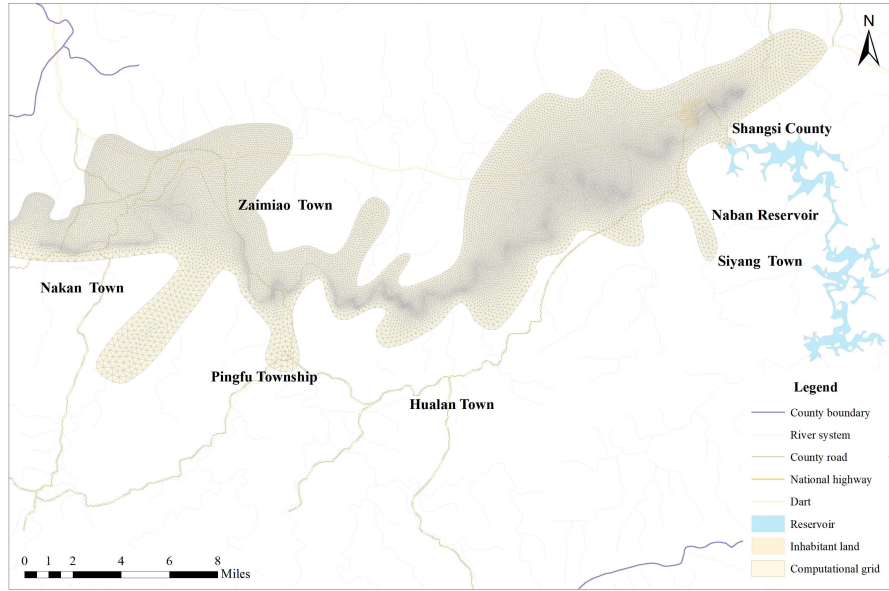


Figure 4. Calculation of grid area

Table 4. One-dimensional model of upstream and downstream boundaries

River Name	Starting Mileage	End Mileage (m)	Upstream Boundary Conditions	Downstream Boundary Conditions
Ming River	0	73350	Flooding process of Naban Reservoir at each frequency	Cross-sectional water level - flow relationship

3.3 Model Calibration and Validation

3.3.1 Model calibration approach

Field studies of the Ming River basin and Naban Reservoir were conducted, and hydrological data were subsequently collected and analyzed to determine and validate the model rates. By assimilating the typical annual flood conditions of both the Ming River basin and Naban Reservoir, the parameters of the coupled model were calibrated and validated.

It has been previously indicated that both boundary conditions and riverbed roughness play intricate roles in determining flood evolution uncertainties [36]. Here, streambed roughness refers to the texture of the streambed surface, which inherently influences energy losses during floodwater progression. The roughness of the one-dimensional model parameters was calculated using flood control engineering data from the Ming River and adjacent waterways. Initial values for the roughness of each segment were provisionally established between 0.03 and 0.05.

The two-dimensional hydrodynamic model was simulated with a temporal resolution of one second. The process of designating roughness was informed by land-use data and remote sensing imagery from the flanks of the Ming River. The roughness file was represented using Manning's value. Different land types were ascribed specific roughness values as detailed in Table 5.

Table 5. Flood risk area roughness table

Lower Pad	Place of Residence	Trees	Dry Field	Water Field	Roads	Open Space	River
Roughness (n)	0.07	0.065	0.06	0.05	0.035	0.035	0.025 – 0.035

3.3.2 Model validation

For the validation phase, measured flood data from the Ming River, dated 18 September 2014, was utilized (as shown in Figure 5 and Table 6). This data set was sourced from the Naban Reservoir Management Centre. A juxtaposition of the simulated outcomes with the actual measured values exhibited correlation coefficients spanning between 0.945 and 0.986. The observed relative errors were -13.72%, -0.23%, -17.41%, and -15.44%, respectively. Notably, flow values from both simulated and actual measurements remained broadly aligned, and the simulation discrepancies fell within the acceptable error threshold (less than 20%). Consequently, it can be inferred that the developed model is reflective of real-world conditions within the Ming River.

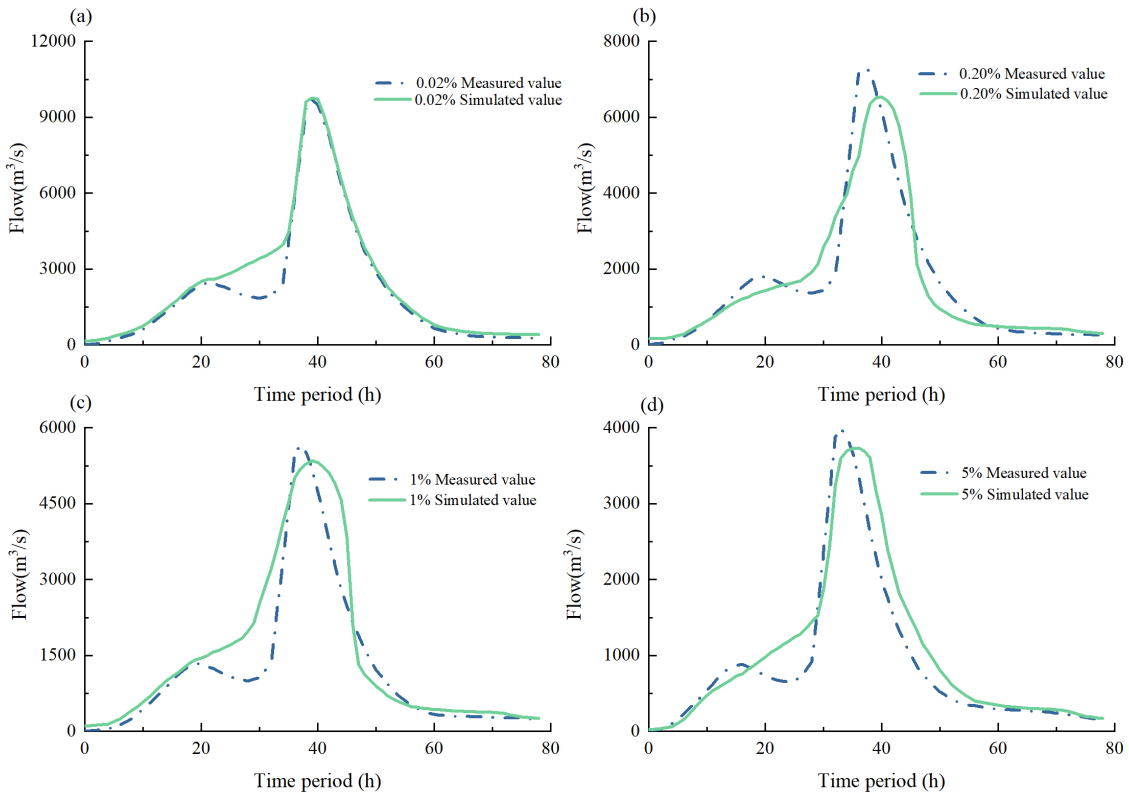


Figure 5. Model validation results

Table 6. Numerical simulation results compared with the measured information

Frequency	Average Measured Flow / $m^3 \cdot s^{-1}$	Average Simulated Flow / $m^3 \cdot s^{-1}$	Absolute Error/ $m^3 \cdot s^{-1}$	Relative Error/ %	Relativity Coefficient R
5000a	2164.89	2461.95	297.06	-13.72	0.986
500a	1630.68	1634.43	3.75	-0.23	0.946
100a	1240.73	1502.29	261.56	-17.41	0.945
20a	882.04	1018.23	136.19	-15.44	0.955

4 Analysis of Simulation Results

4.1 Assessment of Flood Disaster Impacts

Based on the design, construction, safety evaluation report, and risk-mitigation data of Naban Reservoir, as well as observations from the reservoir site, two potential flood emergencies were identified: over-standard flooding events and dam-break floods. Historical data from Naban Reservoir floods informed the consideration of three operational scenarios: floods with return periods of 5000 years, 500 years, and 100 years. For the dam-break flood, the most adverse reservoir conditions associated with a 5000 years check flood, and the implications of unusual high-water level leakage were taken into account. The flood evolution process in the Ming River's lower reaches was assessed based on three parameters: peak flood level, maximum water depth, and flood arrival time. The subsequent sections delve into the flood impacts associated with the Naban Reservoir.

Model simulations provided the peak flood level, maximum water depth, and flood arrival time progressions for the Ming River under the conditions of Naban Reservoir's flood discharge and dam break (refer to Figure 6). As delineated in subgraph (a) of Figure 6, a general decline in the peak flood water level of Naban Reservoir along the Ming River was noted for both the overtopping release and dam-break flood events. The largest peak flood water level was observed during a dam breach at the 5000 years calibration level, while the smallest occurred during the 100 years flood event. This disparity is attributed to the maximal flow during the former dam breach and the minimal flow during the latter flood release. Remarkably, the end peak flood levels for all four emergencies were convergent, suggesting minimal threat to the inhabitants and their properties along the river, from Naban Reservoir's dam site to the Ming River's Shangsi section.

The maximum water depths, from the dam site to the terminating cross-section, were tabulated, as displayed in subgraph (b) of Figure 6. A generalized declining trend in maximum water depth was observed for all flood emergencies in the Naban Reservoir. However, a slight increase in maximum water depth was discerned 20,000 m from the dam site for the three overtopping flood conditions, attributable to the more subtle topography and consequently slower floodwaters, resulting in increased water levels.

According to subgraph (c) of Figure 6, four scenarios were examined for flood occurrences near the Naban Reservoir dam site. The order of flood front arrivals were: a dam breach at the 5000 years check level, a 5000 years flood, a 500 years flood, and a 100 years flood. It was observed that the flood from the 5000 years check level breach was the earliest to manifest, whereas the 100 years flood was the latest. This trend suggests a correlation between the flood's onset and its velocity, with higher flow rates corresponding to faster velocities and earlier flood front arrivals.

The simulation outcomes from the aforementioned scenarios indicate that, within the Ming River Basin of the Naban Reservoir, the most significant water disaster impact stems from a dam failure during the 5000-year calibration flood. This situation presents the most considerable challenge to the flood prevention and mitigation capacities of the downstream areas. When subjected to a dam failure of the 5000-year calibrated flood, the peak flood level attained was 199.12m, with inundation depths reaching up to 30.57m in downstream regions. This flood event propagated rapidly from the reservoir site, eventually submerging the downstream area.

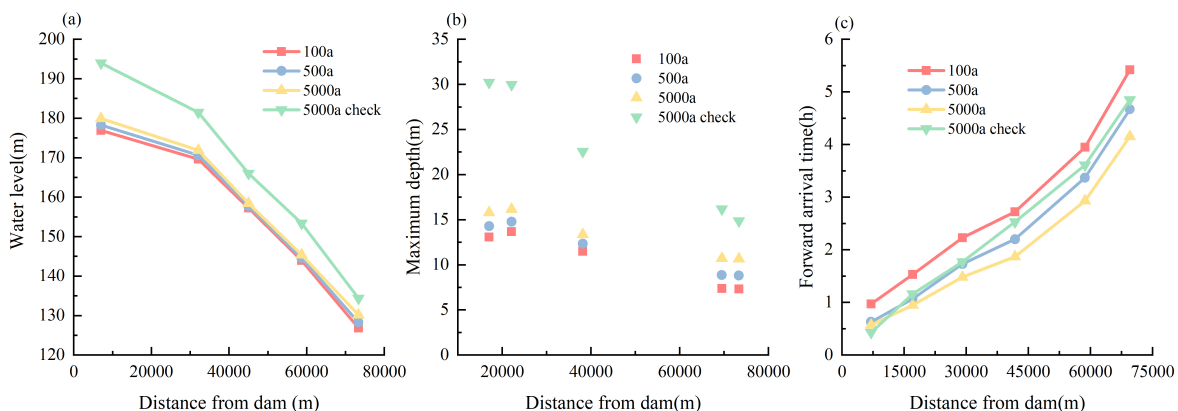


Figure 6. Model validation results

4.2 Flood Risk Analysis

Within the context of the Ming River basin pertaining to the Naban Reservoir, the populace affected by the inundation range under various flooding frequencies was quantified (as depicted in Figure 7). The data revealed that for flood occurrences with return periods of 100 years, 500 years, and 5000 years during standard release, 10,668,

28,491, and 33,664 individuals were affected respectively. A significant portion of this population was located in Siyang town, with the urban sector being the most impacted.

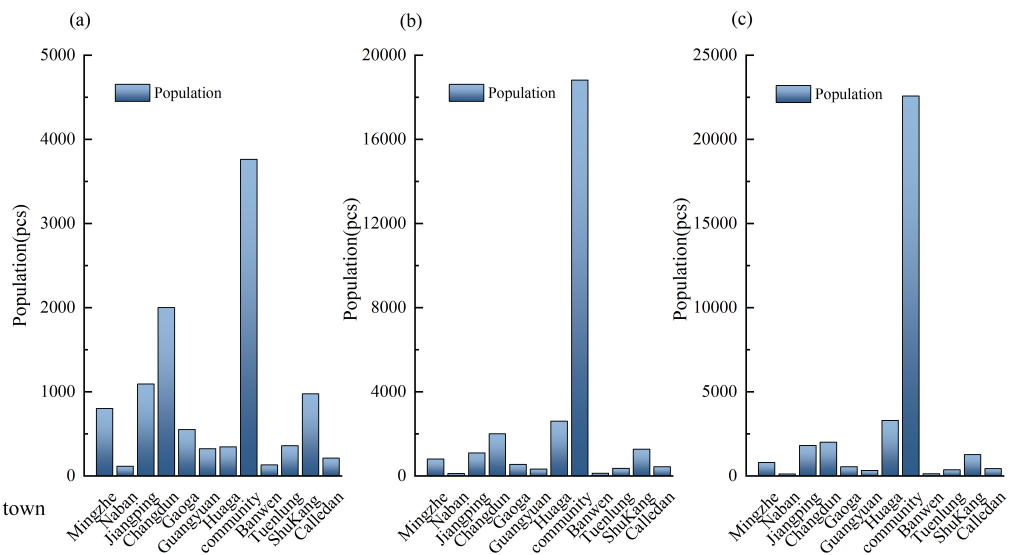


Figure 7. Distribution of populations affected during 100-year, 500-year, and 5000-year flood scenarios

In the unfortunate event of a dam failure at the calibration level within the Naban Reservoir, key parameters, such as the inundation depth, flood flow rate, and flood front arrival time, were assessed downstream (refer to Figures 8, 9, and 10). The inundation depth serves as a pertinent metric for flood risk assessment, facilitating the categorization of water hazard levels based on depth measurements. When subjected to a dam breach at a 5000-year calibration level, the volume of water released was found to be 864.38 million m³. The resultant inundated area was 83.12 km², excluding river zones. Depths of inundation varied from 5 m to 15 m, affecting a land area of 39.90 km². The peak inundation depth varied between 11.28 m and 30.57 m over an area of 14.56 km². The primary areas of inundation were identified downstream of both the Naban and Nianlun Reservoirs, especially at confluences with rivers like the Tuopin, Baobao, and Phoenix. This inundation affected an estimated 100,000 individuals and submerged around 210,000 mu of arable land. Dam failure would result in catastrophic impacts, especially in regions downstream of the Shangsi and Zaimiao basins. Notably, the town of Siyang in Shangsi County, situated approximately 4 km linearly from the dam, was highlighted as being at substantial risk.

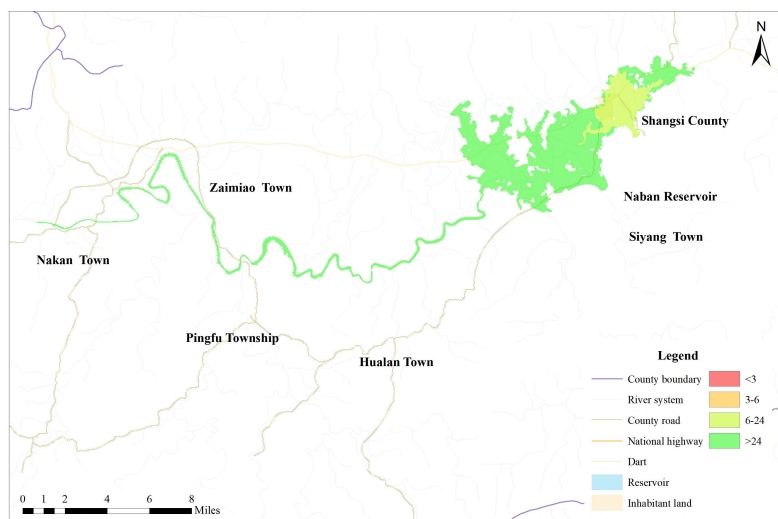


Figure 8. Inundation depth map following a breach at calibration flood level

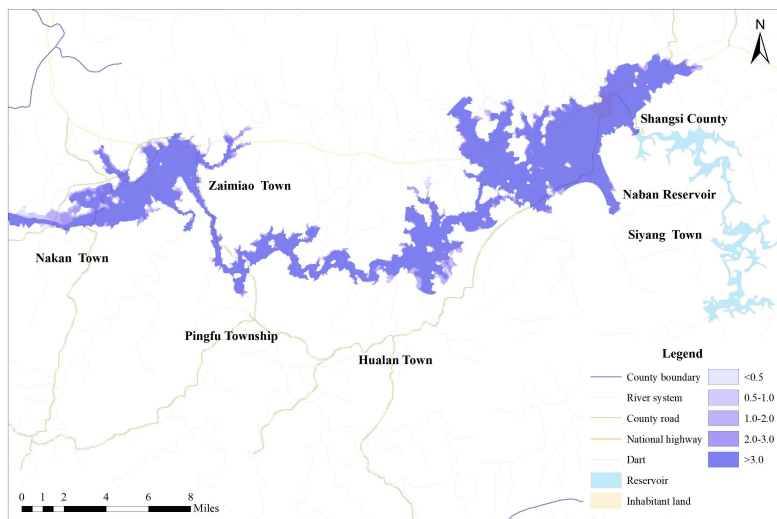


Figure 9. Flow rate map at calibrated flood level breach

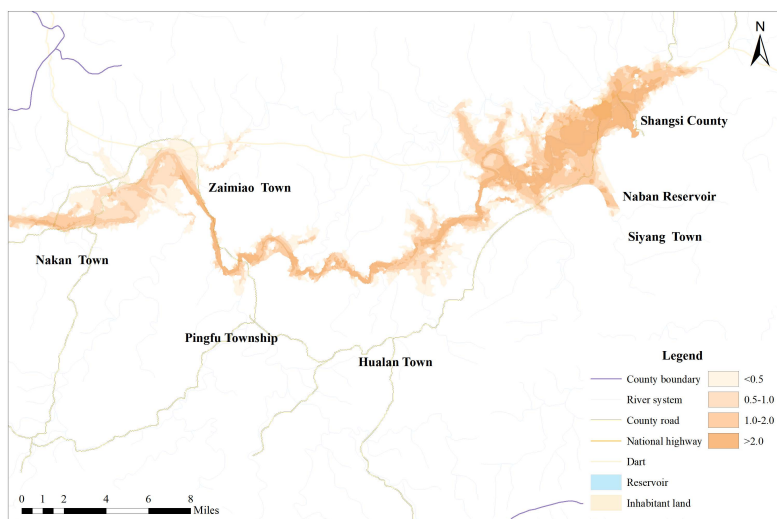


Figure 10. Arrival time of flood front following dam failure

The analysis of the flood front's arrival time during a dam breach at the 5000-year calibration level (illustrated in Figure 10) demonstrated that waters quickly inundated the areas downstream of Nianlun Reservoir along the Tuopin River. Siyang town, located along the Ming River, was the initial region to experience the flood impacts with a response time of less than 0.5 hours. Conversely, in regions downstream of the Dinggou and Baibao rivers, flood front arrival times in Siyang town and Callan town ranged between 0.5 to 1 hour. For areas in Siyang near the Baibao River and in the downstream sections of Dinggou, flood front arrival times extended from 1 to 3 hours. Given the rapid progression of the flood, evacuation and property relocation measures would face stringent time constraints. It is imperative to establish a swift response and dispatch mechanism, amplifying residents' awareness of protective measures and emergency responses to maximize the preservation of lives and property.

4.3 Proposed Emergency Measures for Flood Disaster Safety Management

Based on the outcomes derived from model simulations, several strategic measures are advocated for enhancing the safety management of Nabán Reservoir.

- (1) Risk analyses related to reservoir water disasters should be conducted proactively. Potential safety concerns

for the Naban Reservoir ought to be detected and addressed with early warning systems to enable timely interventions.

(2) The structural integrity of the reservoir, especially components that might harbor latent vulnerabilities, should be rigorously evaluated. Documentation of these assessments should be systematically maintained and disseminated at consistent intervals.

(3) Given that the flood front's approach to the downstream area is typically recorded within a three-hour window, it is imperative that a diversified communication strategy be employed. Information dissemination through public broadcasts, television news, mobile text alerts, and online platforms can expedite the notification process. Such methods can effectively maximize the available time frame for safe evacuations.

(4) In the face of imminent disasters, the seamless operation of communication channels becomes paramount. Collaborations with communication departments might be necessitated to deploy emergency communication apparatus and ensure uninterrupted connectivity in the vicinity of the reservoir.

(5) Logistical preparations are vital for executing large-scale evacuations. Provisions should be made to offer sustenance and support, especially in locales likely to face power or water outages.

(6) Emphasis should be placed on raising the flood disaster awareness and preparedness levels of the resident population. By ensuring that residents are well-informed and educated on best practices, the adverse impacts of potential flood disasters can be substantially mitigated.

5 Conclusion

This study focused on the Ming River basin of the Naban Reservoir located in the Guangxi Zhuang Autonomous Region. Utilizing a one-two-dimensional coupled model, a flood model of the Naban Reservoir was constructed. Investigations were centered on flood evolution, flood inundation by discharge, and flood inundation resultant from dam failure during instances of 100-year, 500-year, and 5000-year floods in regular discharge, alongside a 5000-year calibration water level scenario.

Key findings from this research are as follows:

(1) Roughness calibration was achieved using observed data from the Ming River. For river roughness values ranging between 0.025 and 0.035, with a settlement value of 0.07 and an open space roughness of 0.035, deviations between the coupled model's predicted and observed values were minimal, indicating high accuracy. All simulation outcomes remained within the permissible error range.

(2) Minimal impact on the downstream shoreline was observed during routine flooding of Naban Reservoir across varied frequencies. However, a significant alteration was noted when the reservoir underwent a 5000-year calibration level dam failure. In this scenario, the dam failure volume was estimated at 864.38 million m³, leading to an inundated area of 83.12 km². The compromised zone spanned 39.90 km², with a maximum inundation depth ranging from 11.28 m to 30.57 m, impacting an area of 14.56 km². Predominantly, the inundated regions were located downstream of the reservoir and its adjacent river. Over 100,000 residents were affected, and an estimated 210,000 mu of arable land was submerged. Such a dam failure would inflict catastrophic damage to the downstream Shangsi and Zaimiao Basins, with Siyang Town being the most susceptible.

(3) Variability in the flood front's arrival time was recorded across different regions following the dam's failure. Siyang Town emerged as the initial recipient of the flood, presenting an alarmingly short emergency response time of fewer than 0.5 hours. Absence of prior alerts poses challenges in ensuring comprehensive and safe evacuations. Inhabitants along both sides of the downstream Ming River are advised to relocate before the impending flood. Authorities are urged to devise a swift response and dispatch mechanism, while concurrently enhancing residents' cognizance of emergency protocols to curtail water disaster threats.

(4) Through the integration of MIKE11 and MIKE21 models, a flood warning system for the Naban Reservoir was developed. This system enabled real-time flood predictions and advance warnings, augmenting the reservoir's disaster prevention and mitigation potential. It is posited that the findings from the Naban Reservoir flood model can be extrapolated to other small and medium-sized reservoirs, offering valuable data insights and scholarly benchmarks for flood disaster risk investigations in similar environments.

(5) Given the intricate nature of enacting flood prevention and mitigation policies, this study abstains from delving into detailed procedural implementations. Subsequent research endeavors might explore government strategies in streamlining response mechanisms, elevating public awareness surrounding flood prevention, and pinpointing optimal timelines for early evacuations.

Data Availability

Not applicable. The data in this paper was also used in other scientific projects where the data was not applicable because of confidentiality agreements.

Conflicts of Interest

The authors declare that they have no conflicts of interest.

References

- [1] S. Kalimisetty, A. Singh, D. R. K. H. Venkata, V. R. V, and V. Mahamood, “1D and 2D model coupling approach for the development of operational spatial flood early warning system,” *Geocarto Int.*, vol. 37, no. 15, pp. 4390–4405, 2021. <https://doi.org/10.1080/10106049.2021.1886335>
- [2] Z. Wu, Y. Shen, H. Wang, and M. Wu, “An ontology-based framework for heterogeneous data management and its application for urban flood disasters,” *Earth Sci. Inform.*, vol. 13, no. 2, pp. 377–390, 2020. <https://doi.org/10.1007/s12145-019-00439-3>
- [3] L. Ma, J. Hou, D. Zhang, J. Xia, B. Li, and L. Ning, “Numerical modeling of two-dimensional flood evolution with coupled outburst evolution,” *J. Water Res.*, vol. 50, no. 10, pp. 1253–1267, 2019.
- [4] Y. C. Zheng, J. Z. Li, Y. T. Rong, Y. Du, and P. Feng, “Quantification of spatial and temporal distribution of rainfall and its application to the classification of flood processes,” *J. Water Res.*, vol. 53, no. 05, pp. 560–573, 2022.
- [5] S. Pathak, M. Liu, D. Jato-espino, and C. Zevenbergen, “Social, economic and environmental assessment of urban sub-catchment flood risks using a multi-criteria approach: A case study in Mumbai City, India,” *J. Hydrol.*, vol. 591, p. 125216, 2020. <https://doi.org/10.1016/j.jhydrol.2020.125216>
- [6] W. Ge, Y. Jiao, M. Wu, Z. Li, T. Wang, W. Li, Y. Zhang, W. Gao, and P. V. Gelder, “Estimating loss of life caused by dam breaches based on the simulation of floods routing and evacuation potential of population at risk,” *J. Hydrol.*, vol. 612, p. 128059, 2022. <https://doi.org/10.1016/j.jhydrol.2022.128059>
- [7] S. Harrigan, E. Zsoter, H. Cloke, P. Salamon, and C. Prudhomme, “Daily ensemble river discharge reforecasts and real-time forecasts from the operational Global Flood Awareness System,” *Hydrol. Earth Syst. Sc.*, vol. 27, no. 1, pp. 1–19, 2023.
- [8] G. Lu and X. Zhang, “Prospects for research on the application of high technology in water conservancy industry,” *Water Res. Hydropower Technol.*, vol. 32, no. 1, pp. 53–56, 2001. <https://doi.org/10.3969/j.issn.1000-0860.2001.01.013>
- [9] R. Chen, B. Han, L. Zhao, Y. Zhang, and Y. Cao, “Study on water hazard risk in Maqi River Basin, Puyang City under extreme rainfall conditions,” *Water Res. Hydropower Technol.*, vol. 53, no. 06, pp. 34–43, 2022.
- [10] A. H. Thielen, P. Bubeck, A. Heidenreich, J. Keyserlingk, L. Dillenardt, and A. Otto, “Performance of the flood warning system in Germany in July 2021 - insights from affected residents,” *Nat. Hazards Earth Syst.*, vol. 23, no. 2, pp. 973–990, 2023. <https://doi.org/10.5194/nhess-23-973-2023>
- [11] H. Q. Zhao, L. Zhou, R. Zhao, Z. Li, and Z. Qi, “Simulation of flooding process in plain area watershed based on MIKE coupled model,” *China Rural Water Conser. Hydropower*, no. 7, pp. 97–102, 2022.
- [12] D. J. Moisès and O. Kunguma, “Strengthening Namibia’s flood early warning system through a critical gap analysis,” *Sustain.*, vol. 15, no. 1, p. 524, 2022. <https://doi.org/10.3390/su15010524>
- [13] A. Rostami, M. Akhoondzadeh, and M. Amani, “A fuzzy-based flood warning system using 19-year remote sensing time series data in the google earth engine cloud platform,” *Adv. Space Res.*, vol. 70, no. 5, pp. 1406–1428, 2022. <https://doi.org/10.1016/j.asr.2022.06.008>
- [14] T. Yasmin, K. Khamis, A. Ross, S. Sen, A. Sharma, D. Sen, S. Sen, W. Buytaert, and D. M. Hannah, “Brief communication: Inclusiveness in designing an early warning system for flood resilience,” *Nat. Hazards Earth Syst.*, vol. 23, no. 2, pp. 667–674, 2023. <https://doi.org/10.5194/nhess-23-667-2023>
- [15] Z. Wu, Y. Shen, H. Wang, and M. Wu, “Urban flood disaster risk evaluation based on ontology and Bayesian Network,” *J. Hydrol.*, vol. 583, p. 124596, 2020. <https://doi.org/10.1016/j.jhydrol.2020.124596>
- [16] Q. Wang, Y. Peng, J. Wu, X. Wang, D. Zou, J. Zhang, and Z. Wang, “Analysis of the impact of urban superstandard flooding based on Mike’s coupled model,” *Hydropower Energy Sci.*, vol. 39, no. 8, pp. 94–98, 2021.
- [17] S. L. Harlan, M. J. Sarango, E. A. Mack, and T. A. Stephens, “A survey-based assessment of perceived flood risk in urban areas of the United States,” *Anthropocene*, vol. 28, p. 100217, 2019.
- [18] A. Petrosell, J. Florek, D. M Iłyński, L. Książek, and A. Walega, “New insights on flood mapping procedure: Two case studies in Poland,” *Sustain.*, vol. 12, no. 20, p. 8454, 2020. <https://doi.org/10.3390/su12208454>
- [19] S. H. Mahmoud and G. T. Yew, “Multi-criteria approach to develop flood susceptibility maps in arid regions of the Middle East,” *J. Clean. Prod.*, vol. 196, pp. 216–229, 2018.
- [20] Y. Sado-Inamura and K. Fukushi, “Empirical analysis of flood risk perception using historical data in Tokyo,” *Land Use Policy*, vol. 82, pp. 13–29, 2019. <https://doi.org/10.1016/j.landusepol.2018.11.031>
- [21] W. J. Li, K. R. Lin, G. T. Zhao, T. Lan, X. H. Chen, H. W. Du, and H. Y. Chen, “Risk assessment and sensitivity analysis of flash floods in ungauged basins using coupled hydrologic and hydrodynamic models,” *J. Hydrol.*, vol. 572, pp. 108–120, 2019. <https://doi.org/10.1016/j.jhydrol.2019.03.002>
- [22] A. S. Toosi, S. Doulabian, E. G. Tousi, G. H. Calbimonte, and S. Alaghmand, “Large-scale flood hazard

- assessment under climate change: A case study," *Ecol. Eng.*, vol. 147, p. 105765, 2020. <https://doi.org/10.1016/j.ecoleng.2020.105765>
- [23] Z. Cui, S. Guo, J. Wang, J. Zhang, and R. Zhou, "Research on probabilistic flood process forecasting based on hybrid deep learning model," *J. Water Res.*, pp. 1–10, 2023.
- [24] X. Zhang, B. Duan, S. He, and Y. Lu, "Simulation study on the impact of ecological water replenishment on reservoir water environment based on Mike21-Taking Baiguishan reservoir as an example," *Ecol. Indic.*, vol. 138, p. 108802, 2022. <http://dx.doi.org/10.1016/j.ecolind.2022.108802>
- [25] M. Morales-hernández, M. B. Sharif, A. Kalyanapu, S. K. Ghafoor, T. T. Dullo, S. Gangrade, S. C. Kao, M. R. Norman, and K. J. Evans, "TRITON: A Multi-GPU open source 2D hydrodynamic flood model," *Environ. Model. Softw.*, vol. 2021, p. 105034, 2021. <https://doi.org/10.1016/j.envsoft.2021.105034>
- [26] G. Chen, J. Hou, N. Zhou, S. Yang, Y. Tong, F. Su, L. Huang, and X. Bi, "High-resolution urban flood forecasting by using a coupled atmospheric and hydrodynamic flood models," *Front. Earth Sci.*, vol. 8, 2020. <https://doi.org/10.3389/feart.2020.545612>
- [27] M. Jahandideh-tehrani, F. Helfer, H. Zhang, G. Jenkins, and Y. Yu, "Hydrodynamic modelling of a flood-prone tidal river using the 1D model MIKE HYDRO River: Calibration and sensitivity analysis," *Environ. Monit. Assess.*, vol. 192, no. 2, p. 97, 2020.
- [28] L. Shu, P. A. Ullrich, and C. J. Duffy, "Simulator for Hydrologic Unstructured Domains (SHUD v1.0): Numerical modeling of watershed hydrology with the finite volume method," *Geosci. Model Dev.*, vol. 13, no. 6, pp. 2743–2762, 2020. <https://doi.org/10.5194/gmd-13-2743-2020>
- [29] H. Xiao and J. G. Vasconcelos, "Evaluating curve number implementation alternatives for peak flow predictions in urbanized watersheds using SWMM," *Water*, vol. 15, no. 1, p. 41, 2022. <https://doi.org/10.3390/w15010041>
- [30] E. Janicka and J. Kanclerz, "Assessing the effects of urbanization on water flow and flood events using the HEC-HMS model in the Wirynka River Catchment, Poland," *Water*, vol. 15, no. 1, p. 86, 2022. <https://doi.org/10.3390/w15010086>
- [31] L. Yang, J. Li, A. Kang, S. Li, and P. Feng, "The effect of nonstationarity in rainfall on urban flooding based on coupling SWMM and MIKE21," *Water Resour. Manag.*, vol. 34, no. 4, pp. 1–17, 2020.
- [32] J. Barreiro, F. Santos, F. Ferreira, R. Neves, and J. S. Matos, "Development of a 1D/2D urban flood model using the open-source models SWMM and MOHID land," *Sustain.*, vol. 15, no. 1, p. 707, 2022. <https://doi.org/10.3390/su15010707>
- [33] T. Z. Wang, Y. H. Wang, S. Ma, M. Z. Zhao, L. N. Zhang, Z. C. Xue, Y. Ren, and R. Sun, "MIKE FLOOD coupling model-based flood inundation risk analysis: A case of a science city in Beijing," *Water Res. Hydropower Technol.*, vol. 53, no. 7, pp. 1–17, 2022. <https://doi.org/10.13928/j.cnki.wrahe.2022.07.001>
- [34] L. Lu, X. Pan, and L. Zhang, "Validation of MIKE FLOOD model in flood simulation of Qinghe River basin in Beijing," *Water Res. Hydropower Technol.*, vol. 52, no. S2, pp. 157–163, 2021.
- [35] S. Jiang and Y. Wu, "Comparative analysis of flood control capacity of Nandu River based on MIKE 11 and HEC-RAS," *China Rural Water Conserva. Hydropower Technol.*, no. 2, pp. 46–49, 2014.
- [36] J. Wang, J. Zhao, T. Zhao, and H. Wang, "Partition of one-dimensional river flood routing uncertainty due to boundary conditions and riverbed roughness," *J. Hydrol.*, vol. 608, p. 127660, 2022.